

DEM analysis of granular crushing during simple shearing

Sihong Liu, Yishu Wang & Chaomin Shen

To cite this article: Sihong Liu, Yishu Wang & Chaomin Shen (2017): DEM analysis of granular crushing during simple shearing, Marine Georesources & Geotechnology, DOI: [10.1080/1064119X.2017.1349846](https://doi.org/10.1080/1064119X.2017.1349846)

To link to this article: <http://dx.doi.org/10.1080/1064119X.2017.1349846>



Accepted author version posted online: 21 Aug 2017.
Published online: 21 Aug 2017.



[Submit your article to this journal](#)



Article views: 29



[View related articles](#)



[View Crossmark data](#)



DEM analysis of granular crushing during simple shearing

Sihong Liu, Yishu Wang, and Chaomin Shen

College of Water Conservancy and Hydropower, Hohai University, Nanjing, China

ABSTRACT

In this study, simple shear tests on breakable polydisperse granular materials were simulated using two-dimensional discrete element method (DEM). A new technique of generating polydisperse DEM samples with a smooth and continuous particle size distribution curve was proposed. A modified breakage criterion was introduced to reflect the contact force anisotropy of particles in the numerical sample. The simulation results showed that during the simple shearing, grain crushing in the sample mainly occurred in the contraction process and decreased gradually when the sample began to dilate. As the shearing proceeded to a larger strain, the grain crushing tended to a stable value. This grain crushing trend was in accordance with the evolution of the average normal contact forces of particles in the sample during shearing. The average normal contact forces of potential breakage particles increased in the contraction process and decreased in the dilatancy process. A decrease in the average normal contact forces of potential breakage particles resulted in the decrease in grain crushing during the later stage of shearing.

ARTICLE HISTORY

Received 28 February 2017
Accepted 28 June 2017

KEYWORDS

DEM; granular crushing;
microscopic structure;
simple shear

Introduction

Due to its rewarding advantages, such as flexibility, a high capacity to absorb seismic energy and adaptability to various foundation conditions, granular material is widely used in the coast reclamation works and embankment structures, such as piling and foundations. As a result of some potential defects, microcracks in granular materials develop and particles are easily crushed during loading process. The crushing of large particles into small ones results in the changes in gradation, influencing the mechanical and hydraulic behaviors of the granular materials. Therefore, grain crushing is one of the inevitable problems when studying the mechanical behavior of granular materials.

Many investigations have been conducted on grain crushing, mainly through laboratory tests and numerical simulations. From laboratory tests, it has been found that the factors, such as the particle strength and angularity, porosity, particle size distribution, stress level and stress path, etc., influence the grain crushing significantly (Hardin 1985; Fedá 2002; Fatemiaghda et al. 2016). Several quantitative indexes characterizing the grain crushing have been proposed from particle size distributions before and after the tests (Marsal 1967; Hardin 1985; Lade, Yamamuro, and Bopp 1996; Einav 2007). Different findings on the evolution of grain crushing have also been obtained from the laboratory tests. The drained triaxial compression tests on dense Cambria sand by Lade, Yamamuro, and Bopp (1996) indicated that Hardin's relative breakage parameter B_r tended to a relatively stable value at high confining pressures. However, ring shear and shear box tests on carbonate sand and quartz sand by Luzzani and Coop (2002) showed that particle breakage continued to very large strains, with no evidence of a stable grading being reached within the range of strains used.

The numerical simulations for the grain crushing are usually carried out using discrete element method (DEM), which was first developed by Cundall for rock mass problems and later applied to granular materials by Cundall and Strack (1979). DEM can provide a simple way to visualize the evolution of grain crushing. It is also possible to interpret grain crushing from a microscopic view based on the simulation results. Usually, there are two approaches in DEM numerical simulation to consider particle breakage:

- The first approach is to treat each particle as a porous agglomerate (cluster) built by bonding smaller particles. These agglomerates can disaggregate during the simulations. This approach has been used by Nakata, Hyodo, et al. (2001), McDowell and Harireche (2002), Cheng, Nakata, and Bolton (2003), and Wang and Yan (2013).
- The second approach is to replace the particles fulfilling a predefined failure criterion with an equivalent group of smaller particles. This approach has been used by Tsoungui et al. (1999), Lobo-Guerrero and Vallejo (2005), Vallejo and Lobo-Guerrero (2005), and Ben-Nun and Einav (2008, 2010).

Based on the second approach, the grain crushing is further investigated in this paper through the DEM numerical simulation of simple shear tests, which allows the investigation in a relatively large shear strain. A new way to generate the DEM sample with a continuous gradation is developed. The breakage criterion is modified so that it can adapt to the continuous gradation. The evolution of grain crushing with the change in volumetric strain during simple shearing is investigated.

Generation of a DEM specimen with continuous gradation

Most granular materials occurring in nature and engineering application are composed of particles with a broad range of

sizes. Some research indicates that a uniformly graded granular material exhibits more crushing than a well-graded material with the same maximum particle size (Lade, Yamamuro, and Bopp 1996; Nakata, Hyodo et al. 2001). To reflect a more realistic grain crushing phenomenon, the generation of a specimen with a broad range of sizes is important in DEM simulations. At present, the DEM specimens generated are mostly composed of particles with some specific sizes. For example, Jiang, Konrad, and Leroueil (2003) proposed a multi-layer with under compaction method to generate homogeneous DEM specimens, in which the particle size distribution (PSD) was first discretized into several “classes,” defined over subintervals, and the particles in each class had the same size. Voivret et al. (2007) proposed a space-filling method to build densely packed specimens of prescribed polydispersity for DEM studies, in which a similar particle size generation technique was adopted. Since the current methods as mentioned above cannot generate the DEM specimen with a smooth and continuous PSD, a new technique is presented in this study, in which the PSD is replaced with a probability density function (PDF).

In the probability theory, a PDF $p(x)$ is a function that describes the relative likelihood for this random variable to take on a given value. For a random variable X varying in the range $[x_1, x_2]$, if the probability of X falling within the range $[x_1, x_2]$ is denoted as $P(x)$, the probability of X on interval $[x, x + \Delta x]$ is $P(x + \Delta x) - P(x)$. The PDF of a random variable X is then given by

$$p(x) = \lim_{\Delta x \rightarrow 0} \frac{P(x + \Delta x) - P(x)}{\Delta x} = \frac{dP}{dx} \quad (1)$$

The PSD is often represented by the cumulate mass distribution (CMD) of the particles. In this study, we assume the CMD of particles is represented by a continuous function $\Phi(D)$ of particle diameters D varying in the range $[D_1, D_2]$, as the solid curve shown in Figure 1. By definition, the percentage of particles over the interval $[D, D + dD]$ is $d\Phi$. The number of particles with diameter D can be calculated by

$$dN(D) = \frac{M d\Phi}{\rho V_D} \quad (2)$$

where M is the total mass of the specimen; ρ is the particle density; and V_D is the volume of the particle with diameter D . For a circular particle, $V_D = \pi D^2/4$. Hence, the probability of the particles with diameters over the interval $[D, D + dD]$ is given by

$$dP = \frac{dN(D)}{N} \quad (3)$$

where N is the total number of particles in the specimen, and can be calculated by integration of Eq. (2), $N = \int_{D_1}^{D_2} (M/\rho V_D) d\Phi$. Therefore, the PDF $p(D)$ corresponding to the particle with diameter D can be calculated as follows

$$p(D) = \frac{dP}{d} = \frac{1}{N} \frac{dN(D)}{dD} = \frac{\frac{d\Phi}{dD}}{\left(V_D \int_{D_1}^{D_2} \frac{d\Phi}{V_D} \right)} \quad (4)$$

The dotted curve in Figure 1 is the $p(D)$ derived from the $\Phi(D)$. The value of $p(D)$ decreases with the increase in particle diameter.

In this study, the Von Neumann's (1951) acceptance-rejection method is adopted to generate the variable X fulfilling the $p(x)$. The generation procedure is summarized as follows:

1. Assume X varying from x_1 to x_2 , that is, $X \in [x_1, x_2]$.
2. Choose a parameter λ that $\lambda p(x) \leq 1, \forall x \in [x_1, x_2]$.
3. Generate uniformly distributed pseudo-random numbers r_1 and r_2 that $r_1, r_2 \in (0, 1)$. Let $y = x_1 + (x_2 - x_1)r_1$.
4. Compare r_2 and $\lambda p(y)$. If $r_2 \leq \lambda p(y)$, let $x = y$ and output x . Otherwise, abandon r_1 and r_2 , then return to step (3).

Repeat the above procedure to generate the random number sequence x_1, x_2, \dots, x_n . The generated random number sequence corresponds to different particle diameters and fulfills the given PSD.

Figure 2 gives the entire procedure of generating the DEM specimen based on the PDF.

In this study, based on the PSD of a real coarse granular material (Figure 3a), a DEM specimen for simulating the simple shear test is generated using the proposed method, as shown in Figure 3b. The specimen consists of 1,650 circular particles with maximum and minimum diameters of 60 and 2.5 mm, respectively. It is in a $30 \times 30 \text{ cm}^2$ rectangular area bounded by four rigid walls and has an initial void ratio of 0.15.

Breakage criterion

In this study, grain crushing is simulated by replacing one particle that fulfills a predefined failure criterion with an equivalent group of smaller particles, that is, the second approach mentioned above. Lobo-Guerrero and Vallejo (2005) and Vallejo and Lobo-Guerrero (2005) proposed a failure criterion that was based on the magnitude of the loads applied to the particle, the particle coordination number, and the particle size. It was pointed out that only particles with coordination number N_c equal to or smaller than 3 were possible to be broken using this failure criterion. They thought

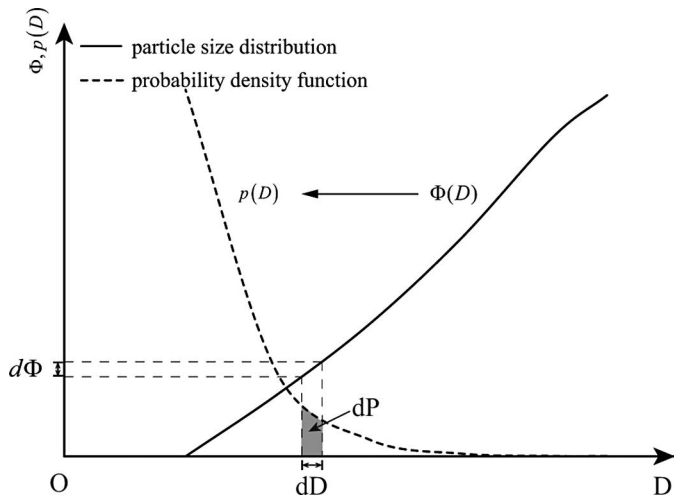


Figure 1. PSD curve and the corresponding PDF curve of grain diameters. Note: PSD, particle size distribution; PDF, probability density function.

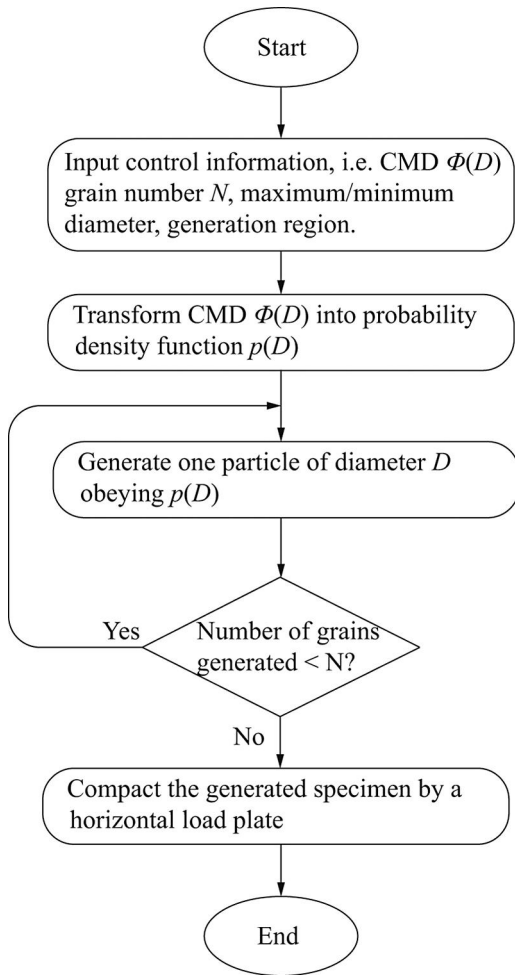
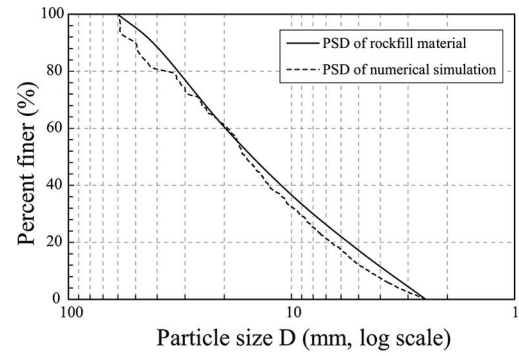


Figure 2. Flowchart for specimen preparation procedure.

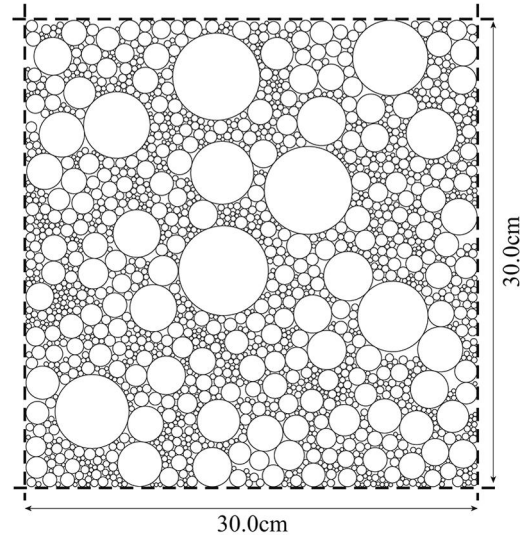
that the large particles surrounded by small grains ($N_c > 3$) did not easily break because the small grains confined the large ones, producing a hydrostatic state of stress. The experimental studies illustrated that grain crushing was related to the contact force between particles and the state of confinement (Lade, Yamamuro, and Bopp 1996). However, (Alaei and Mahboubi 2012) thought that the coordination number N_c could not be a suitable parameter to represent the particle confinement because it does not encompass the magnitude or orientation of the contact forces. To consider the confinement in the breakage criterion, they suggested that the contact force orientation anisotropy (A_f) was preferred to the coordination number N_c .

As some larger particles in the generated DEM specimen with a continuous PSD are surrounded with several smaller particles, their coordination numbers N_c are probably greater than 3. To study the grain crushing for widely graded specimen, the parameter A_f suggested by Alaei and Mahboubi (2012) was introduced into the failure criterion proposed by Lobo-Guerrero and Vallejo (2005) and Vallejo and Lobo-Guerrero (2005). The parameter A_f is defined as the maximum value of $F_{(\theta)}$

$$F_{(\theta)} = \frac{f_{\theta}}{\sum f_{\theta}}, A_f = (F_{(\theta)})_{\max} = \frac{(f_{\theta})_{\max}}{\sum f_{\theta}} \quad (5)$$



(a)



(b)

Figure 3. DEM specimen and its particle size distribution. (a) PSD of the specimen. (b) DEM numerical specimen. Note: DEM, discrete element method; PSD, particle size distribution; PDF, probability density function.

where $F_{(\theta)}$ is described as the fraction of the total contact forces that are applied within the orientation interval $\Delta\theta = 20^\circ$; f_{θ} is the algebraic sum of the contact forces oriented at the angular interval between θ and $\theta + \Delta\theta$, and $\sum f_{\theta}$ is the algebraic sum of all the contact forces.

To clearly explain this concept, a single particle with contact forces and components of Eq. (5) is shown in Figure 4. During DEM cycling, A_f was calculated for all particles and only the particles with $A_f > 0.33$ have the capability of breakage. For the potential breakage particles, the crushing strength criterion proposed by Guerrero and Vallejo was further adopted to judge their crushability. The details of the Guerrero and Vallejo's crushing strength criterion are referred to the literature (Lobo-Guerrero and Vallejo 2005; Vallejo and Lobo-Guerrero 2005). Therefore, in this paper, the single particle can break into a group of eight fragments only if (a) the microstructure parameter A_f is more than 0.33, and (b) the tensile stress induced by the applied contact forces exceeds the defined crushing strength.

The breakage configuration that particles are allowed to break into a group of eight fragments with three different sizes was based on the research results of Tsoungui et al. (1999), which has been used in the DEM simulation by Lobo-Guerrero and Vallejo (2005). However, the breakage

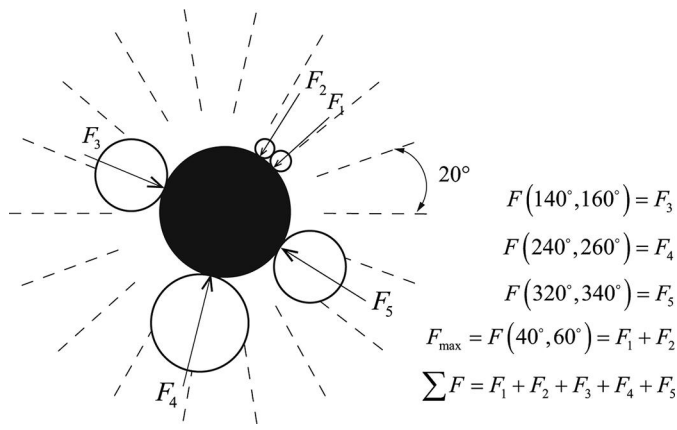


Figure 4. A single particle confined by smaller particles and contact force orientation anisotropy.

configuration implemented in DEM by Lobo-Guerrero and Vallejo (2005) (Figure 5c) does not satisfy the mass conservation. The mass difference between one parent crushed particle and the eight replacing fragments is 1/6 mass of the parent particle. We conserve the mass by enlarging the fragments in proportion to their sizes, as illustrated in Figure 5d. The artificial enlargement of the fragments results in the overlaps and thereby the artificial contact forces between the fragments/particles in the breakage area. To resolve this problem, supplementary DEM cycling with a reduced time step was executed under the condition of constant external loading until the calculation tends to be stable.

Numerical simulation of simple shear test

The simple shear test is numerically carried out on the specimen shown in Figure 3b. As shown in Figure 6, the simple

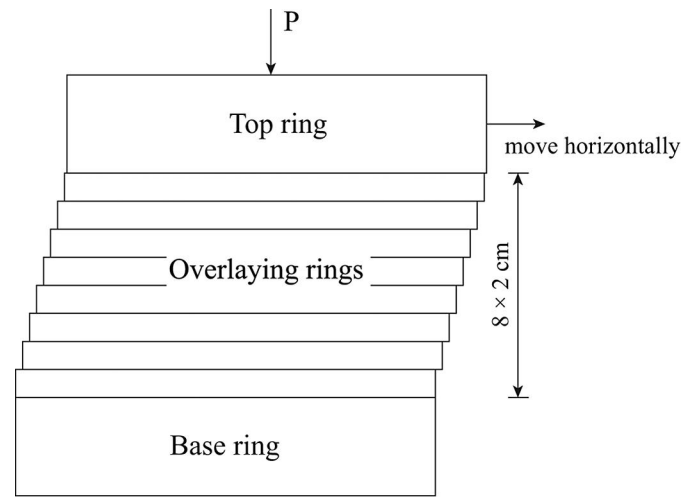


Figure 6. Schematic diagram of simple shear test.

shear mode is motivated by overlaying rings because it can build boundary conditions with a nonlinear lateral deformation, which is important for large shearing deformation as pointed out by Bauer and Huang (1999). In the numerical simulation, a prescribed constant vertical pressure is applied on the top ring, and the shear strain of the specimen is produced by moving the top ring laterally at a low speed while the base ring is fixed. Although the generated DEM specimen has a height of 30 cm, the region of the simple shear mode is limited to be 16 cm (Figure 6) because we want to study the grain crushing in the shear strain as large as possible.

Explicit discrete element method is used in this study: The simulation involves cyclic calculations. At the time instant t , the penetrations between particles are identified and the contact forces are updated, using the incremental force–displacement relationships. The total unbalanced forces and the momentum of each particle are then obtained by summing up its contact forces; new translational and angular accelerations are evaluated using Newton’s second law. Numerical integration of the accelerations, using a small time increment Δt , gives the velocities at the instant $t + \Delta t/2$, which are numerically integrated again to provide the displacement from t to $t + \Delta t$. Having obtained the new configuration of the assemblies, another cycle of calculations is repeated until the process in question terminates. Figure 7 shows the scheme of the cyclic calculations. A DEM code based on this scheme was programmed using Fortran language, which has been used to study the wetting-induced collapse deformation (Fu, Chen, and Liu 2012) and the yield function based on the microscopic structures (Liu et al. 2015).

The parameters involved in the DEM simulation are the normal and tangential stiffness k_n and k_s , the normal and tangential damping η_n and η_s , the inter-particle friction coefficient μ , the particle density ρ , and the tensile strength of a particle with a radius of 1 mm $\sigma_{\max 1 \text{ mm}}$, which are listed in Table 1. The normal and tangential stiffness k_n and k_s are determined on the assumption that the inter-particle contact is envisioned as a set of elastic springs uniformly distributed over a rectangular cross section as proposed by Potyondy and Cundall (2004). The stiffness k_n of a particle can be

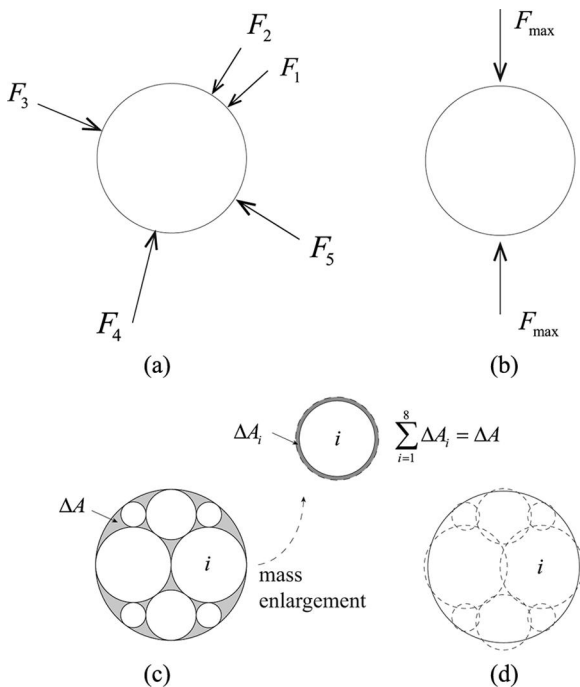


Figure 5. Particle breakage criterion. (a) Particle forces. (b) Force simplified method. (c) Particle breakage. (d) Area correction.

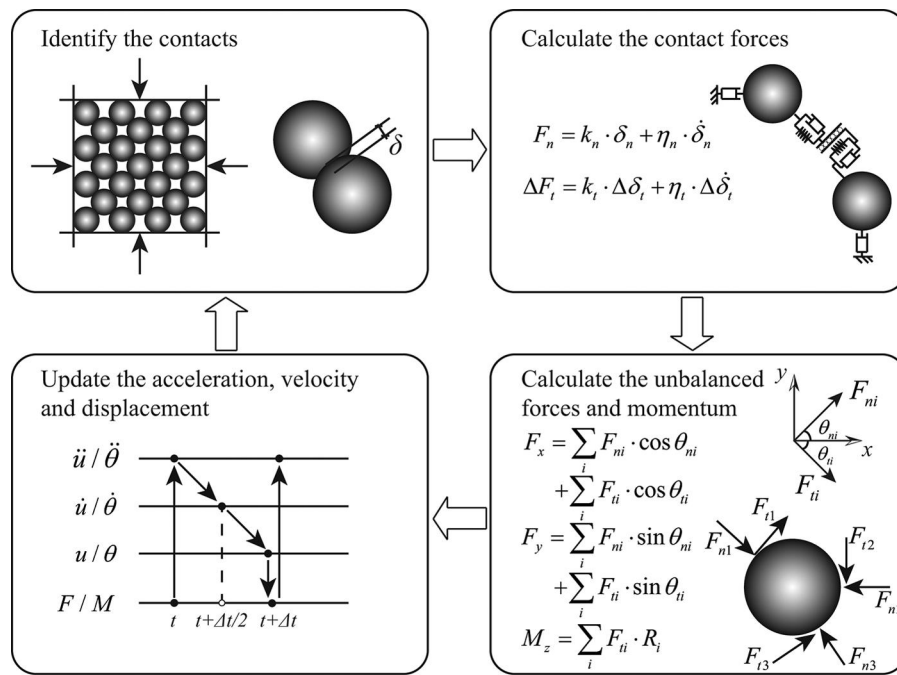


Figure 7. Scheme of cyclic calculations in explicit DEM. Note: DEM, discrete element method.

calculated by $k_n = 2tE_c$ ($t = 1$ for 2D), where E_c is the Young's moduli of the particles and is selected as 17.5 MPa. The damping η is calculated using the formula $\eta = 2\sqrt{km}$, where k is the contact stiffness and m is the average mass of the contacting particles in the specimen. The inter-particle friction coefficient μ is set to be 0.5 (Minh and Cheng 2013). The particle density ρ of 1.900 kg/m³ is the representative value of the soil. The tensile strength of an individual particle is related to its particle size and can be calculated by $\sigma_{\max}(r) = \sigma_{\max 1 \text{ mm}}/r$, where $\sigma_{\max 1 \text{ mm}}$ is the tensile strength of a particle with a radius of 1 mm and is assumed to be 5.0×10^6 Pa (Lobo-Guerrero and Vallejo 2005; Nakata, Kato, et al. 2001). It should be pointed out here that as the study in this paper focuses mainly on the particle breakage during the simple shearing instead of the strain localization, the contact law between particles in the simulation is simplified to be linear without rotational moments.

Figure 8a and b shows the relationships for the simulated shear stress ratio τ/σ_y and volumetric strain versus the shear strain of crushable and uncrushable materials under vertical stresses of 200 and 400 kPa, respectively. The shear stress of the specimen is calculated from the horizontal components of the contact forces of the particles along the bottom of the top ring. The shear strain and volumetric strain are defined as the horizontal and the vertical displacements of the top ring

divided by the height of the simple shear region (16 cm). As depicted in Figure 8a, the ratios of shear stress to vertical stress under the two different vertical stresses of 200 and 400 kPa tend to be a stable value of about 0.14 at a large shear strain. The fluctuation of the shear stress ratio can be observed, probably resulting from the relatively small number of particles in the calculated DEM specimen. Compared to the uncrushable materials, the fluctuation of the shear stress ratios of the crushable materials is more pronounced, especially at the vertical stress of 400 kPa. The volumetric strains of the specimen contract initially and then dilate to a relatively stable value at a large shear strain under both vertical stresses. For crushable materials, larger volumetric contraction takes place. Figure 9 gives the experimental results of the simple shear tests on a crushable silt mudstone under the vertical stress of 200 and 400 kPa using a large-scale simple shear test device with eight-staged shearing rings (Kong 2014). The similar patterns of the stress-strain behaviors between the experimental results and the numerical results can be observed.

Analysis of particle breakage

Figure 10 gives the PSD curves at the end of shearing with the final shear strain of 35% under vertical stresses of 200 and 400 kPa, respectively. It is observed that the PSD curves are broadened because of particle breakage and the PSD shifts toward the area of finer grain sizes, especially under the vertical stress of 400 kPa. At the end of shearing, the particle breakage leads to the increase in the particles in the specimen from the original 1,650–2,329 and 2,476 under the vertical stress of 200 and 400 kPa, respectively.

To quantify the particle breakage, the index of Hardin's relative breakage Br was used, which was based on the relative position of the current PSD from an initial PSD and an

Table 1. Input parameters for the DEM calculations.

Parameters	Value
Normal stiffness k_n (N/m ²)	3.5×10^7
Tangential stiffness k_s (N/m ²)	1.2×10^7
Normal damping η_n (N · s/m ²)	2.7×10^3
Tangential damping η_s (N · s/m ²)	1.6×10^3
Particle friction (μ)	0.5
Particle density ρ (kg/m ³)	1900
Tensile strength of the reference particle $\sigma_{\max 1 \text{ mm}}$ (Pa)	5.0×10^6

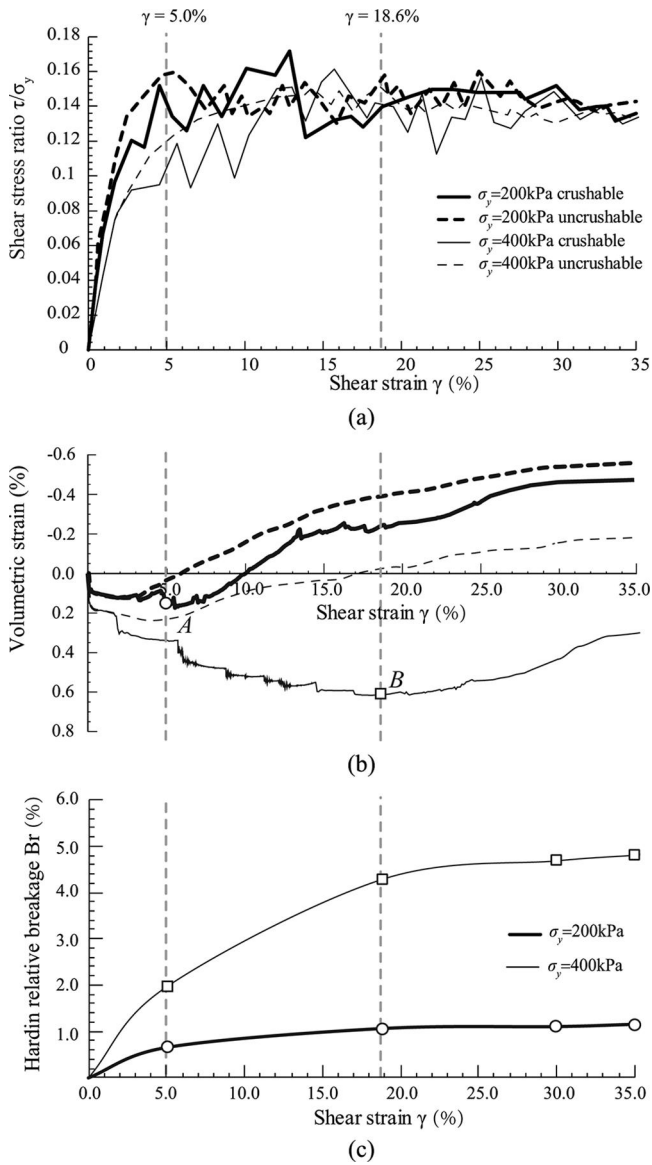


Figure 8. Numerically simulated stress–strain–breakage relationships under shearing. (a) Relationships between shear stress ratio and shear strain. (b) Relationships between volumetric strain and shear strain. (c) Relationships between breakage index and shear strain.

arbitrary cutoff value of “silt” particle size (of 0.074 mm) (Hardin 1985). Figure 8c shows the evolution of Hardin’s relative breakage Br during shearing obtained from the numerical simulation. Compared with the evolution of volumetric strain, the following findings can be observed:

1. The relative breakage Br increases more significantly at the beginning of the shearing and its evolution rate decreases as the shearing continues. The value of the relative breakage Br under the vertical stress of 400 kPa is larger than that under the vertical stress of 200 kPa.
2. Under the vertical stress of 200 kPa, the volumetric strain of the specimen changes from contraction to dilatation at the shear strain of about 5% (point A as indicated in Figure 8b). Before and after point A, the increments of the relative breakage Br are 0.65 and 0.49%, respectively. That is to say, the particle breakage during the contraction process accounts for 56.8% of the total shearing process.

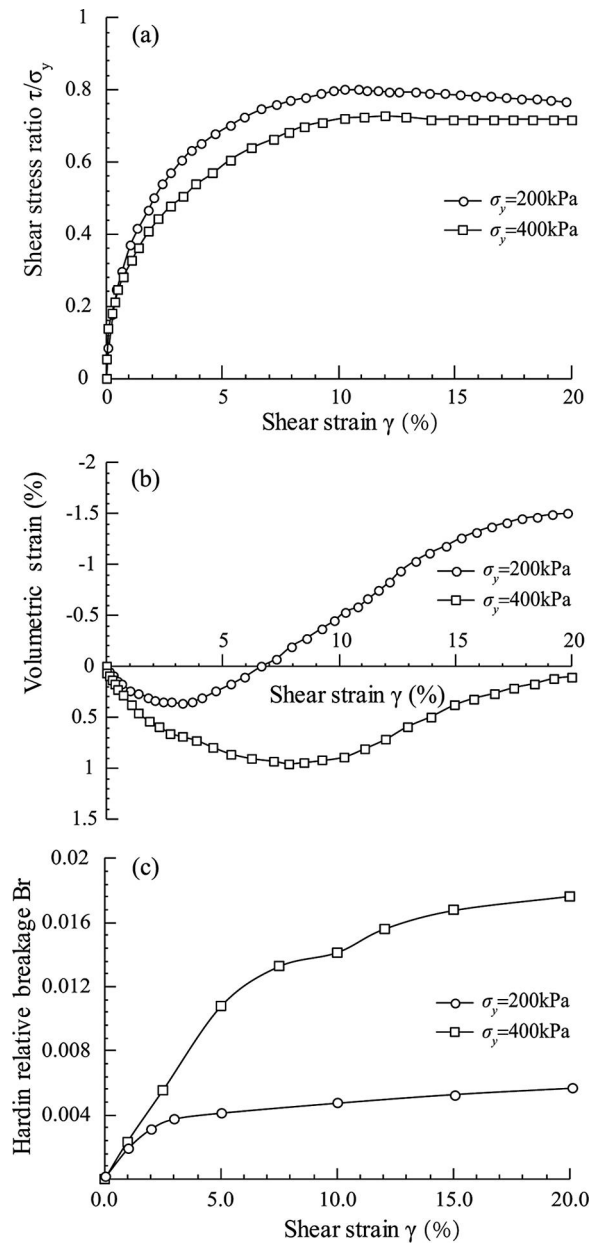


Figure 9. Experimental stress–strain–breakage relationships of a crushable silt mudstone under shearing. (a) Relationships between shear stress ratio and shear strain. (b) Relationships between volumetric strain and shear strain. (c) Relationships between breakage index and shear strain.

3. Under the vertical stress of 400 kPa, the volumetric strain of the specimen is overall contractive, with a slight dilatation observed after the shear strain of 18.6% (point B). The relative breakage Br reaches up to 4.30% before the shear strain of 18.6% and a small increment of 0.52% is observed after the point B.

From these observations, it may be concluded that particle breakage occurs mainly during the contraction process and the increased fragmentation is small during the dilatation process.

Some snap shots are shown in Figure 11 at different values of shear strain under vertical stress of 200 and 400 kPa. The breakage particles are marked in solid black circles. As the shearing process started, the particles experience crushing. When shearing under vertical stress of 200 kPa, the crushing

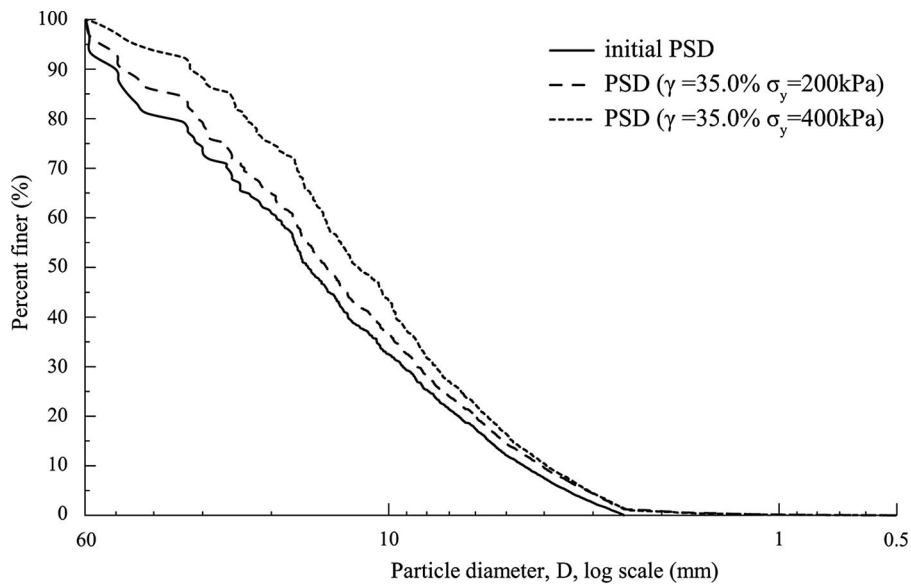
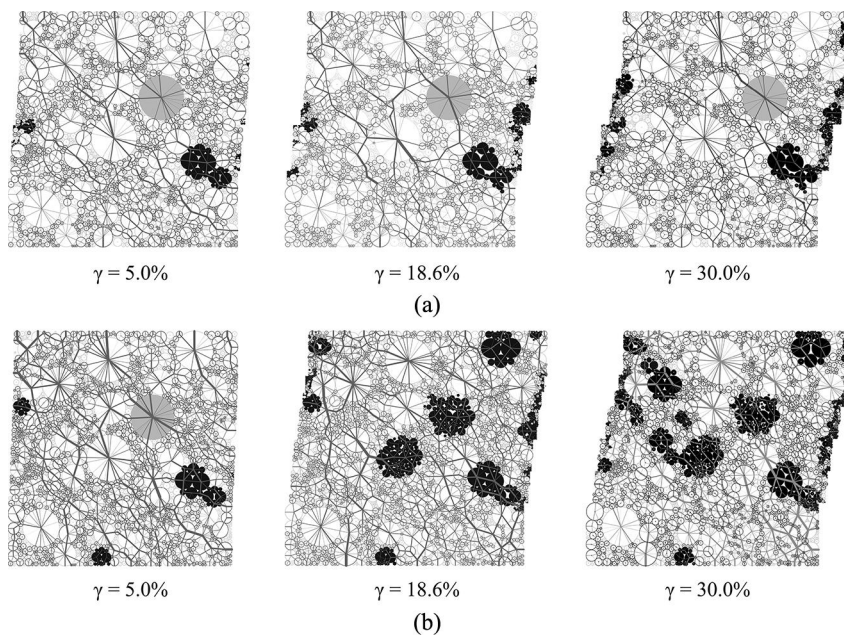


Figure 10. Ultimate PSD curves under different vertical stresses.

occurred mainly on the left and right boundaries. When the vertical stress increased to 400 kPa, the bigger particles inside the specimen began to crush and endured secondary breakage. Figure 11 also shows the evolution of force chains. The magnitude of contact forces is related to the thickness of the force chains. The thicker the force chains, the larger the contact forces.

To gain more insight into the crushing process, we analyze the evolution of contact forces of a representative particle (the solid grey circle in Figure 11) during shearing under two

vertical stresses. Figure 12 shows that at the beginning of the shearing, the contact forces of the particle do not show a clear anisotropy under the two vertical stresses. As the shearing proceeds, the anisotropy of contact forces becomes pronounced in a certain direction. Under $\sigma_y = 200$ kPa, the representative particle does not break at the shear strain of 35.0%, where the maximum normal contact force F_{\max} is 11.5 kN and the neighboring contact forces are relatively small with $A_f < 0.33$. However, under $\sigma_y = 400$ kPa, the particle breaks when the shear strain reaches 8.48%, where the maximum normal



Note: The solid black circles represent crushing particles; the black line circles represent particles with $A_f > 0.33$; while other particles are marked with light grey. The solid grey circle is a representative particle. The grey line with different thickness represent force chains.

Figure 11. Snap shots of crushing during shearing process. (a) Shearing process under $\sigma_y = 200$ kPa. (b) Shearing process under $\sigma_y = 400$ kPa. Note: The solid black circles represent crushing particles; the black line circles represent particles with $A_f > 0.33$; while other particles are marked with light grey. The solid grey circle is a representative particle. The grey line with different thickness represent force chains.

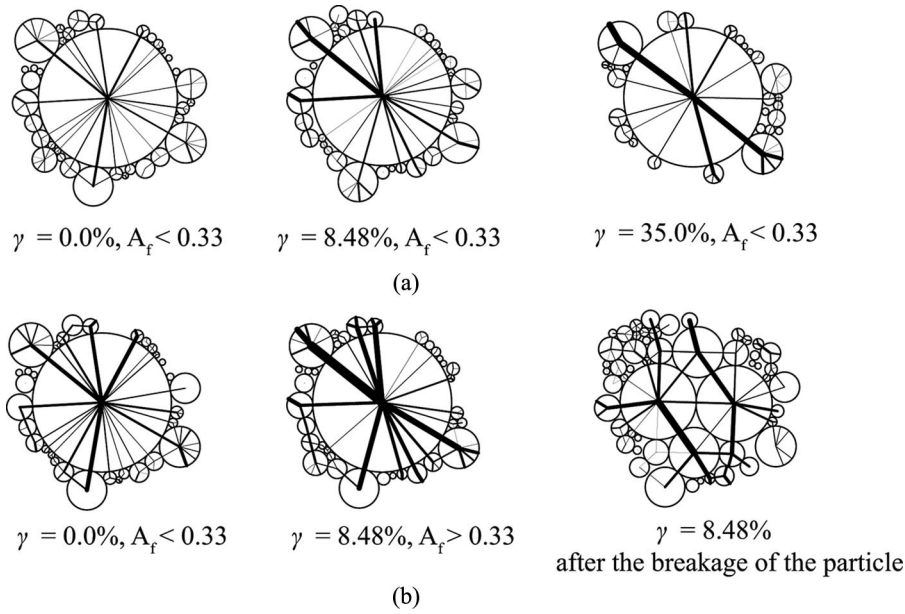


Figure 12. The evolution of force chains of a representative particle during shearing. (a) $\sigma_y = 200$ kPa. (b) $\sigma_y = 400$ kPa.

contact force F_{max} is 15.4 kN and the neighboring contact forces are greater with a significant anisotropy of contact forces ($A_f > 0.33$).

It is believed that particles with $A_f > 0.33$ have the potential to break and contribute to the crushing ability of the granular system. In the following analysis, the particles with $A_f > 0.33$ are marked with black line and are evaluated separately from the rest of the granular medium. Figure 13 shows the evolution of the average normal contact forces of all particles ($A_f > 0$) and the potential breakage particles ($A_f > 0.33$) during shearing under different vertical stresses. Compared with the evolution of particle breakage (Figure 8b) and volumetric strain (Figure 8c), the following can be concluded from Figure 13:

1. The normal contact forces of particles in the sample are correlated with the vertical stress applied. The average normal contact forces of all particles and potential breakage

particles under vertical stress of 400 kPa are almost doubly larger than those under vertical stress of 200 kPa, which result in the different amount of particle breakage under two vertical stresses.

- Under the vertical stress of 200 kPa, the average normal contact force of potential breakage particles begins to endure slight decrease after the shear strain increases to 5%, and a similar pattern occurs under the vertical stress of 400 kPa when the shear strain increased close to 18.6%. The average normal contact forces of all particles both under vertical stress 200 and 400 kPa endure slight increase and tend to be stable, which indicate the shear strain has slight influence on the magnitude of average normal contact forces for all particles.
- Compared with the evolution of volumetric change shown in Figure 8b, it indicates that the average normal contact

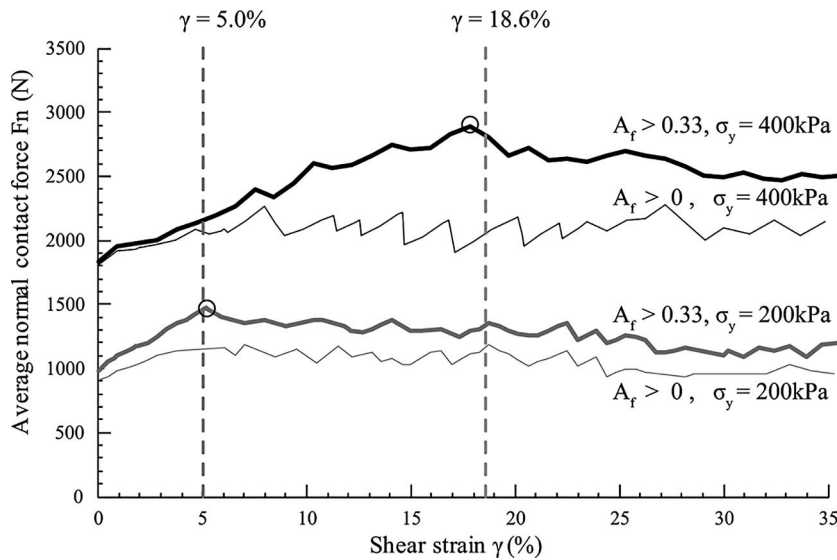


Figure 13. Evolution of average contact forces for the potential breakage particles.

forces between potential breakage particles increase during compression process, and endure decrease when the sample begins to dilate. Particles are more easily to be crushed in the volume contraction stage because the average normal contact forces of potential breakage particles continue increasing, and crushing gradually tends to be stable state in the ultimate dilatation state because the average normal contact force of potential breakage particles decreases when the sample begins to dilate.

4. As the shear strain has slight influence on the magnitude of contact forces and the rotation of contact force will finally stop with the increasing shear strain, the fabric in the sample will tend to be stable state, which indicates a gradual decrease in particle breakage and a stable value of relative breakage index.

Conclusion

The behavior of crushable granular materials was investigated by numerically simulating simple shear experiments on a continuous-graded assembly of circles. Two vertical stresses were applied to the DEM sample to study the evolution of crushing. The main conclusions were drawn as follows:

1. A technique for generating a DEM sample with a continuous distributed PSD curve was proposed to reflect a more realistic granular material with polydisperse particles.
2. A modified breakage criterion was introduced, in which a parameter A_f was adopted to reflect the contact force anisotropy instead of using coordination number, and the mass conservation was guaranteed before and after grain crushing.
3. The simulation results showed that during the simple shearing, the grain crushing in the sample mainly occurred in the contraction process and decreased gradually when the sample began to dilate. As the shearing proceeded to a larger strain, the grain crushing tended to a stable value.
4. The trend of grain crushing during simple shearing was in accordance with the evolution of the average normal contact forces of potential breakage particles in the sample. The average normal contact forces of potential breakage particles increase during the contraction process and tend to be stable in the dilation process. As a result, the amount of grain crushing increases during the contraction process and decreases during the dilation process.

The focus of this study was on the evolution of particle breakage during simple shearing. Our future work will include the effect of initial void ratios on particle breakage and the influence of breakage on the strain localization.

Funding

This research is funded by the National Natural Science Foundation of China (Grant No. 51179059), the Postgraduate Research & Practice Innovation Program of Jiangsu Province (Grant No. KYZZ_0148), the Fundamental Research Funds for the Central Universities (Grant No. 2016B40914), and the China Scholarship Council (No. 201506710031). The supports are greatly appreciated.

References

- Alaei, E., and A. Mahboubi. 2012. A discrete model for simulating shear strength and deformation behaviour of rockfill material, considering the particle breakage phenomenon. *Granular Matter* 14 (6):707–17. doi:10.1007/s10035-012-0367-7.
- Bauer, E., and W. Huang. 1999. Numerical study of polar effects in shear zones. In *Numerical models in geomechanics*, ed. G. N. Pande, S. Pietruszczak, H. F. Schweiger, 133–41. Rotterdam: Balkema.
- Ben-Nun, O., and I. Einav. 2008. A refined DEM study of grain size reduction in uniaxial compression. Proceedings of the 12th International Conference of the International Association for Computer Methods and Advances in Geomechanics (IACMAG), Goa, India, 702–08.
- Ben-Nun, O., and I. Einav. 2010. The role of self-organization during confined comminution of granular materials. *Philosophical Transactions. Series A, Mathematical, Physical, and Engineering Sciences* 368 (1910):231–47. doi:10.1098/rsta.2009.0205.
- Cheng, Y. P., Y. Nakata, and M. D. Bolton. 2003. Discrete element simulation of crushable soil. *Géotechnique* 53 (7):633–41. doi:10.1680/geot.2003.53.7.633.
- Cundall, P. A., and O. D. L. Strack. 1979. A discrete numerical model for granular assemblies. *Géotechnique* 29 (1):47–65. doi:10.1680/geot.1979.29.1.47.
- Einav, I. 2007. Breakage mechanics-part I: theory. *Journal of the Mechanics and Physics of Solids*, 55 (6):1274–1297. doi:10.1016/j.jmps.2006.11.003.
- Fatemiaghda, M., H. Shahnazari, H. R. Karami, and M. Talkhablu. 2016. Effect of texture of carbonate soils in South Iran coasts on aggregate crushing. *Marine Georesources & Geotechnology* 1–13. doi:10.1080/1064119x.2016.1275893.
- Feda, J. 2002. Notes on the effect of grain crushing on the granular soil behaviour. *Engineering Geology* 63 (1–2):93–98. doi:10.1016/s0013-7952(01)00072-2.
- Fu, Z., S. Chen, and S. Liu. 2012. Hypoplastic constitutive modelling of the wetting induced creep of rockfill materials. *Science China Technological Sciences* 55 (7):2066–82. doi:10.1007/s11431-012-4835-4.
- Hardin, B. O. 1985. Crushing of Soil Particles. *Journal of Geotechnical Engineering* 111 (10):1177–92. doi:10.1061/(asce)0733-9410(1985)111:10(1177).
- Jiang, M. J., J. M. Konrad, and S. Leroueil. 2003. An efficient technique for generating homogeneous specimens for DEM studies. *Computers and Geotechnics* 30 (7):579–97. doi:10.1016/s0266-352x(03)00064-8.
- Kong, W. 2014. Experimental study on the mechanical behaviour of rockfill materials during cyclic simple shear tests. Master Thesis, Hohai University.
- Lade, P. V., J. A. Yamamuro, and P. A. Bopp. 1996. Significance of particle crushing in granular materials. *Journal of Geotechnical Engineering* 122 (4):309–16. doi:10.1061/(asce)0733-9410(1996)122:4(309).
- Liu, S., Z. Wang, Y. Wang, L. Wang, and Z. Fu. 2015. A yield function for granular materials based on microstructures. *Engineering Computations* 32 (4):1006–24. doi:10.1108/ec-04-2014-0093.
- Lobo-Guerrero, S., and L. E. Vallejo. 2005. Discrete element method evaluation of granular crushing under direct shear test conditions. *Journal of Geotechnical and Geoenvironmental Engineering* 131 (10):1295–300. doi:10.1061/(asce)1090-0241(2005)131:10(1295).
- Luzzani, L., and M. R. Coop. 2002. On the relationship between particle breakage and the critical state of sands. *Soils and Foundations* 42 (2):71–82. doi:10.3208/sandf.42.2_71.
- Marsal, R. J. 1967. Large scale testing of rockfill materials. *Journal of Soil Mechanics and Foundations Division* 93 (2):27–43.
- McDowell, G. R., and O. Harireche. 2002. Discrete element modelling of yielding and normal compression of sand. *Géotechnique* 52 (4):299–304. doi:10.1680/geot.2002.52.4.299.
- Minh, N. H., and Y. P. Cheng. 2013. A DEM investigation of the effect of particle-size distribution on one-dimensional compression. *Géotechnique* 63 (1):44–53. doi:10.1680/geot.10.p.058.
- Nakata, Y., M. Hyodo, A. F. Hyde, Y. Kato, and H. Murata. 2001. Microscopic particle crushing of sand subjected to high pressure

- one-dimensional compression. *Soils and Foundations* 41 (1):69–82. doi:10.3208/sandf.41.69.
- Nakata, Y., Y. Kato, M. Hyodo, A. F. Hyde, and H. Murata. 2001. One-dimensional compression behaviour of uniformly graded sand related to single particle crushing strength. *Soils and Foundations* 41 (2):39–51. doi:10.3208/sandf.41.2_39.
- Potyondy, D. O., and P. A. Cundall. 2004. A bonded-particle model for rock. *International Journal of Rock Mechanics and Mining Sciences* 41 (8):1329–64. doi:10.1016/j.ijrmms.2004.09.011.
- Tsoungui, O., D. Vallet, and J. C. Charmet. 1999. Numerical model of crushing of grains inside two-dimensional granular materials. *Powder Technology* 105 (1):190–98. doi:10.1016/s0032-5910(99)00137-0.
- Vallejo, L. E., and Lobo-Guerrero, S. 2005. DEM analysis of crushing around driven piles in granular materials. *Géotechnique* 55 (8): 617–23. doi:10.1680/geot.2005.55.8.617.
- Voivret, C., F. Radjai, J. Y. Delenne, and M. S. El Yousoufi. 2007. Space-filling properties of polydisperse granular media. *Physical Review E* 76 (2):1–12. doi:10.1103/physreve.76.021301.
- Von Neumann, J. 1951. 13. Various techniques used in connection with random digits. *Appl. Math Ser* 12:36–38.
- Wang, J., and H. Yan. 2013. On the role of particle breakage in the shear failure behavior of granular soils by DEM. *International Journal for Numerical and Analytical Methods in Geomechanics* 37 (8):832–54. doi:10.1002/nag.1124.